Aging Cell (2012) **11,** pp439–448 Doi: 10.1111/j.1474-9726.2012.00801.x

O-GlcNAcase is essential for embryonic development and maintenance of genomic stability

Yong Ryoul Yang,[1,2] Minseok Song,[3] Ho Lee,[4] Yoon Jeon,[4] Eun-Jeong Choi,[1] Hyun-Jun Jang,[1,2] Hyo Youl Moon,[2,5] Ha-Young Byun,[1,2] Eung-Kyun Kim,[1,2] Dae Hyun Kim,[2] Mi Nam Lee,[1] Ara Koh,[1] Jaewang Ghim,[1] Jang Hyun Choi,[6] Whaseon Lee-Kwon,[2] Kyong Tai Kim,[1] Sung Ho Ryu[1] and Pann-Ghill Suh[1,2]

[1]Division of Molecular and Life Science, Pohang University of Science and Technology, Pohang, Kyungbuk 790-784, Republic of Korea
[2]School of Nano-Biotechnology and Chemical Engineering, Ulsan National Institute of Science and Technology, Ulsan 689-798, Republic of Korea
[3]Department of Psychiatry, Weill Cornell Medical College, New York, NY 10065, USA
[4]Cancer Experimental Resources Branch, National Cancer Center, Goyang-si, Gyeonggi-do 410-769, Republic of Korea
[5]School of Interdisciplinary Bioscience and Bioengineering, Pohang University of Science and Technology, Pohang 790-784, Republic of Korea
[6]Department of Cancer Biology and Division of Metabolism and Chronic Disease, Dana-Farber Cancer Institute, Boston, MA 02115, USA

Summary

Dysregulation of O-GlcNAc modification catalyzed by O-GlcNAc transferase (OGT) and O-GlcNAcase (OGA) contributes to the etiology of chronic diseases of aging, including cancer, cardiovascular disease, type 2 diabetes, and Alzheimer's disease. Here we found that natural aging in wild-type mice was marked by a decrease in OGA and OGT protein levels and an increase in O-GlcNAcylation in various tissues. Genetic disruption of OGA resulted in constitutively elevated O-GlcNAcylation in embryos and led to neonatal lethality with developmental delay. Importantly, we observed that serum-stimulated cell cycle entry induced increased O-GlcNAcylation and decreased its level after release from G2/M arrest, indicating that O-GlcNAc cycling by OGT and OGA is required for precise cell cycle control. Constitutively, elevated O-GlcNAcylation by OGA disruption impaired cell proliferation and resulted in mitotic defects with downregulation of mitotic regulators. OGA loss led to mitotic defects including cytokinesis failure and binucleation, increased lagging chromosomes, and micronuclei formation. These findings suggest an important role for O-GlcNAc cycling by OGA in embryonic development and the regulation of the maintenance of genomic stability linked to the aging process.

Key words: aging; genomic instability; O-GlcNAcase; O-GlcNAcylation; O-GlcNAc transferase.

Introduction

O-GlcNAcylation culminates with UDP-GlcNAc transfer to target proteins in the hexosamine biosynthetic pathway (HSP). O-GlcNAcylation is a post-translational modification that influences fundamental functions of proteins by regulating protein–protein interactions, altering protein stability, and changing protein activity (Torres & Hart, 1984; Hart *et al.*, 2007, 2010). O-GlcNAc addition and removal from the Ser and Thr residues of proteins is catalyzed by O-GlcNAc transferase (OGT) and O-GlcNAcase (OGA), respectively. OGA, a nucleocytoplasmic β-N-acetylglucosaminidase, is a bifunctional protein containing a glycosidase domain at the N-terminus and a putative histone acetyltransferase domain at the C-terminus (Toleman *et al.*, 2004). *OGA* is mapped to the chromosomal region that is associated with Alzheimer's disease and the development of type 2 diabetes in a Mexican population (Lehman *et al.*, 2005). In addition, many studies have directly linked dysregulation of O-GlcNAc cycling to chronic diseases of aging including diabetes, cardiovascular disease, neurodegenerative disorders, and cancer (Hart *et al.*, 2010). Although the cellular and physiological roles of O-GlcNAc cycling have been extensively investigated, how OGA activity is regulated and what the physiological effects are when OGA is dysregulated *in vivo* remain unclear.

Aging is a multifaceted process characterized by genomic instability and epigenetic changes. Maintenance of genomic stability requires accurate segregation of sister chromosomes during mitosis (Draviam *et al.*, 2004; Holland & Cleveland, 2009). OGT is co-localized to the midbody with OGA, kinase, and phosphatase, and it regulates the post-translational status of vimentin during mitosis (Slawson *et al.*, 2005, 2008). Correlatively, a combined glycoproteomic and phosphoproteomic approach identified O-GlcNAcylation and phosphorylation sites on various spindle and midbody proteins, suggesting that the cross talk between O-GlcNAcylation and protein phosphorylation is crucial to the regulation of cell division (Wang *et al.*, 2010). A recent study showed that OGT glycosylates the cell cycle regulator host cell factor-1 (HCF-1) and cleaves HCF-1 to regulate mitosis (Capotosti *et al.*, 2011). Regarding epigenetic changes, histones are O-GlcNAcylated within the nucleosome core, suggesting a crucial role for O-GlcNAc in chromatin remodeling and epigenetic regulation (Sakabe & Hart, 2010; Sakabe *et al.*, 2010). Thus, we speculate that precise control of O-GlcNAc cycling by OGA and OGT is required for the maintenance of genomic stability and epigenetic regulation associated with aging. Moreover, we found that aged tissues have dysregulated O-GlcNAcylation and O-GlcNAc cycling enzymes.

To elucidate the cellular and physiological roles of OGA associated with dysregulation of O-GlcNAcylation, we generated $OGA^{-/-}$ mice. In our study, we found that OGA homozygous null mice showed perinatal lethality with developmental delay. We observed that O-GlcNAcylation level fluctuated during the cell cycle and constitutively elevated O-GlcNAcylation by OGA disruption resulted in an aberrant cell cycle. $OGA^{-/-}$ mouse embryonic fibroblasts (MEFs) displayed genomic abnormalities, followed by cytokinesis defects, and became senescent. Together, these findings indicate that OGA dysregulation might contribute to the mammalian aging process and affect development of age-related chronic diseases.

Results

Increased O-GlcNAcylation and decreased O-GlcNAc cycling enzymes in aged tissues

To investigate how O-GlcNAcylation level is altered in natural aging, we analyzed the levels of O-GlcNAcylation and O-GlcNAc cycling enzymes

Correspondence
Pann-Ghill Suh, Division of Molecular and Life Science, Pohang University of Science and Technology, Pohang, Kyungbuk 790-784, Republic of Korea.
Tel.: +82 52 217 2621; fax: +82 52 217 2609; e-mail: pgsuh@unist.ac.kr

Accepted for publication *17 January 2012*

Aging Cell

in various tissues of 4-month-old and 20-month-old mice. Notably, the relative O-GlcNAcylation level of older mice was significantly higher than that of younger mice in diverse tissues including brain, lung, skin, thymus, testis, and liver. The protein levels of O-GlcNAc cycling enzymes, OGT and OGA, decreased in tissues of older mice (Fig. 1A–D and data not shown). Although lungs from older mice showed no difference in OGA protein level as compared to lungs from younger mice, O-GlcNAcyltion was elevated (Fig. 1B). This result indicates that the consequent elevation of O-GlcNAcylation might be resulted from increased OGT activity or decreased OGA activity, suggesting the importance of the OGT/OGA balance in normal conditions. We suggest that O-GlcNAc cycling is dysregulated in aged tissue, which is caused by abnormality of the OGT/OGA balance. These results raise the possibility that increased O-GlcNAcylation is associated with the normal aging process.

Generation of *OGA*$^{-/-}$ mice and constitutively elevated O-GlcNAcylation in *OGA*$^{-/-}$ embryos

To examine whether the increased O-GlcNAcylation had cellular and physiological relevance to aging, we generated OGA-deficient mice with a gene-trapped embryonic cell line [YTC085; (Stryke *et al.*, 2003)]. 5′-RACE analysis of the fusion transcript confirmed insertion of the gene trap vector in the first intron of *OGA* and identified the insertion site (Fig. S1A,B). *OGA* disruption was confirmed by polymerase chain reaction (PCR) using mouse tail-derived genomic DNA (Fig. S1C). OGA expression was visualized by whole-mount LacZ staining of *OGA*$^{+/-}$ embryos and placentas, confirming the insertion of the gene trap beta-galactosidase reporter allele (Fig. S1D). Embryo sagittal sections and placenta radial sections stained with X-gal at embryonic day (E) 14.5 revealed that OGA expression was particularly high in the brain and in the labyrinth structure of the placenta (Fig. S2A,B). OGA disruption resulted in constitutively elevated O-GlcNAcylation in *OGA*$^{-/-}$ embryos (Fig. 2A).

Perinatal lethality of *OGA* knockout mice

To obtain *OGA*$^{-/-}$ offspring, we crossed male heterozygotes with female heterozygotes. In more than 100 offspring, we failed to identify the homozygous null mutation at the time of weaning, suggesting that OGA loss causes either embryonic or neonatal lethality. We analyzed *OGA*$^{-/-}$ embryos at different gestational stages and found that *OGA*$^{-/-}$ embryos had stunted growth and that mutant neonates died within 1 day of birth (Table 1). *OGA*$^{-/-}$ embryos were significantly reduced in size and body weight compared with wild-type (WT) embryos (Fig. 2B,C). However, histological analysis of *OGA*$^{-/-}$ embryos did not exhibit gross defects, and we failed to observe any anatomical abnormalities at E14.5 (Fig. 2D). To clarify the cause of neonatal lethality, histological analysis was performed. Lungs from WT and *OGA*$^{+/-}$ mice floated in water, while lungs dissected from *OGA*$^{-/-}$ newborns were dense and sank. As expected, lung histology of *OGA*$^{-/-}$ newborns revealed that the alveolar space was markedly reduced (Fig. 2E). Together, these results show that OGA disruption leads to embryonic developmental delay, indicating an important role of OGA in development.

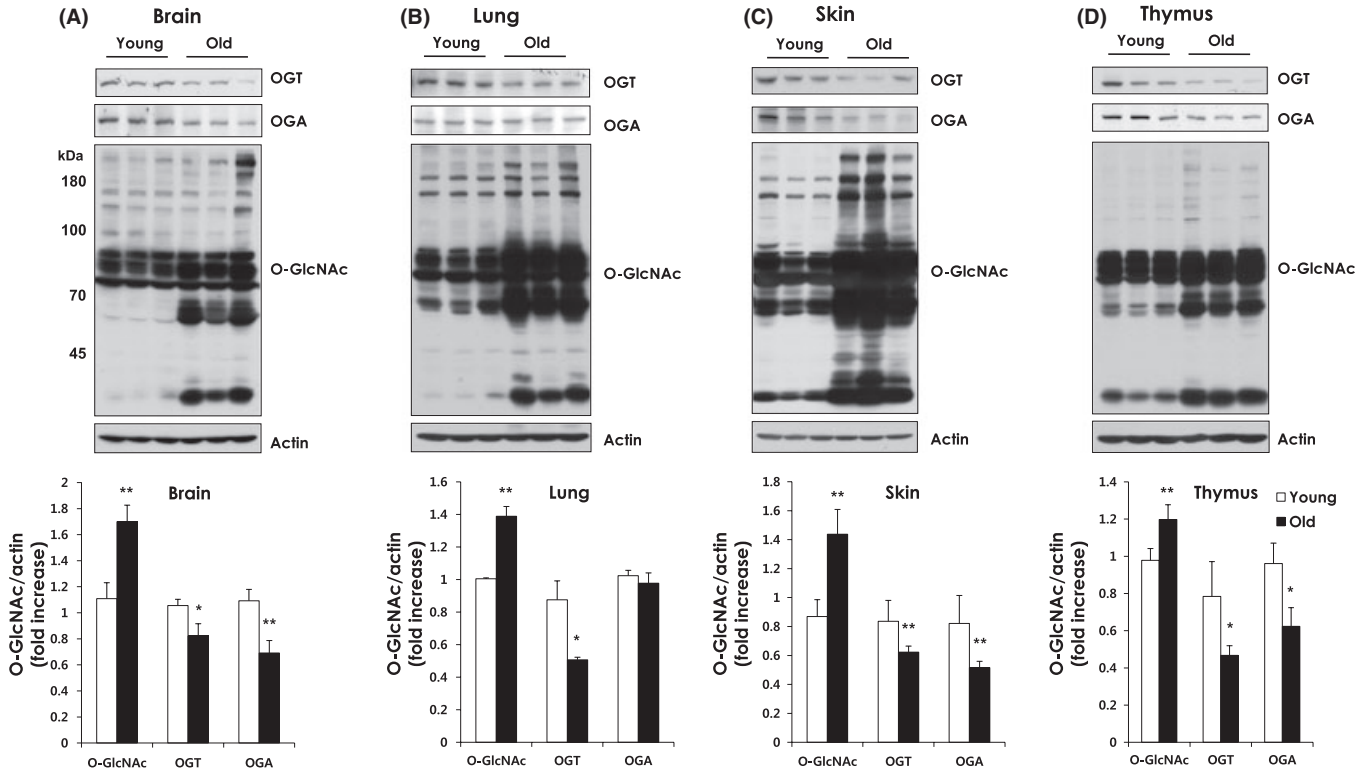

Fig. 1 Increased total O-GlcNAcylation and decreased OGA and OGT protein levels in aged tissue. (A–D) Western blot analysis of OGT, OGA, and O-GlcNAc levels in brain (A), lung (B), skin (C), and thymus (D) of old and young mice. Densitometry was performed on immunoblots. The ratio of O-GlcNAc to β-actin was determined. Error bars represent the S.D. ($n = 3$) and $^{**}P < 0.005$, $^{**}P < 0.05$ (Student's *t*-test).

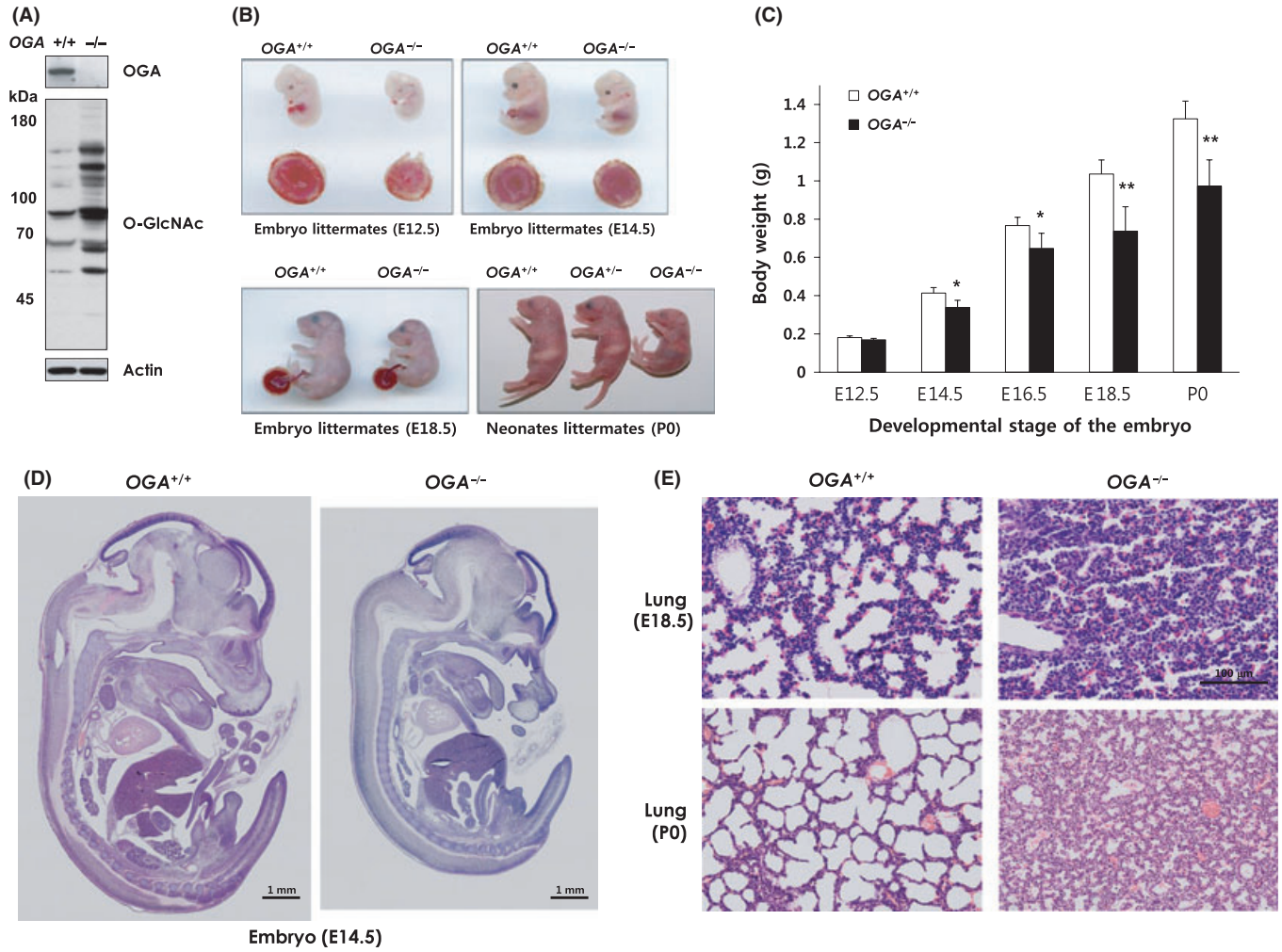

Fig. 2 *OGA*$^{-/-}$ mice die within 1 day of birth and show significantly decreased intrauterine growth. (A) Immunoblot analysis confirmed the loss of OGA protein in the *OGA*$^{+/+}$ and *OGA*$^{-/-}$ whole embryo lysates. (B) Morphology of E12.5, E14.5, E18.5, and neonate littermates. (C) Weight of WT and *OGA*$^{-/-}$ embryos from different gestational periods and neonates. Males and females were pooled. Ten or more embryos per genotype were analyzed. Error bars represent the SD and $^{**}P < 0.005$, $^{*}P < 0.02$ (Student's *t*-test). (D) Sagittal sections of *OGA*$^{+/+}$ and *OGA*$^{-/-}$ E14.5 embryos stained with hematoxylin and eosin. (E) Hematoxylin and eosin staining of *OGA*$^{+/+}$ and *OGA*$^{-/-}$ lungs of E18.5 embryos and P0 neonates (a, pre-alveolar spaces; br, bronchiole).

Proliferative defects in *OGA*$^{-/-}$ MEFs

Reduced body size of whole OGA$^{-/-}$ embryos led us to examine whether the developmental delay could be caused by a cell proliferation defect. To determine whether OGA disruption caused the proliferative defect, we used MEFs isolated from mid-gestation embryos [13.5 days post-conception (dpc)]. We compared cell growth rates at passages (P) 4 and 7 in *OGA*$^{+/+}$ and *OGA*$^{-/-}$ MEFs. *OGA*$^{-/-}$ MEFs exhibited a reduced growth rate compared with WT MEFs (Fig. 3A). OGA knockdown by shRNA also resulted in reduced cell growth in HEK293 cells (Fig. S3A,B). As cellular senescence was characterized *in vitro* by a decline in growth rate, *OGA*$^{-/-}$ MEFs exhibited reduced population-doubling time compared with *OGA*$^{+/+}$ MEFs (Fig. 3B). In addition, enlarged and flattened cell morphology was observed in *OGA*$^{-/-}$ MEFs (data not shown), which are established features of senescence (Dimri *et al.*, 1995). Previous studies have shown that increased O-GlcNAcylation leads to apoptosis (Webster *et al.*, 2009; Rajamani & Essop, 2010). Therefore, we asked whether the reduced growth rate was caused by increased cell death. However, annexin-V staining demonstrated that the decreased cell growth of *OGA*$^{-/-}$ MEFs was not because of apoptosis (Fig. 3B).

Elevation of O-GlcNAcylation in serum-stimulated cell cycle entry

Reduced growth can be attributed to cell cycle defects. Thus, we wondered how O-GlcNAcylation changed during cell cycle progression. We synchronized WT MEFs in G_0 phase by serum starvation and extracted proteins from cells harvested every 4 h after serum stimulation. To dissect cell cycle progression, we analyzed cyclin B1, A, and E levels. The O-GlcNAcylation level significantly increased at 20–24 h post-release, consistent with OGT expression. However, OGA expression was not altered during the cell cycle, suggesting that OGA might be regulated by its enzymatic activity. In accordance with cyclin expression patterns, OGT expression and O-GlcNAcylation were cell cycle-dependent (Fig. 4A). OGT expression level was high in late S phase and peaked at the M phase. The same patterns of OGT expression were confirmed in

Table 1 Genotype of offspring from $OGA^{+/-} \times OGA^{+/-}$ mating after eight generations of backcrossing with C57BL/6 wild-type animals

	No. of offspring with *OGA* genotype of:			
Developmental stage	+/+	$^{+/-}$	$^{+/-}$	Resorbed
E10.5	8	12	7	0
E11.5	9	16	9	2
E12.5	9	13	6	4
E13.5	16	32	12	7
E14.5	18	30	14	7
E15.5	10	18	7	8
E16.5	12	21	8	4
E17.5	10	15	8	3
E18.5	15	26	13	1
Prenatal total (406) (%)	107 (26.10)	183 (44.63)	84 (20.49)	36 (8.78)
P0	48	90	22	
P1	58	131	0	
Prenatal total (349)	106	221	22	

HEK293 cell lines (Fig. 4B). To further confirm the cell cycle-dependent O-GlcNAcylation and OGT expression, we next synchronized WT MEFs in the mitotic phase using nocodazole, an antimitotic drug. We observed similar results showing that the OGT protein level and O-GlcNAcylation peaked at mitotic phase and decreased after release from nocodazole (Fig. 4C). Strikingly, OGT levels and cyclin B1 were similarly altered. Together, these results suggest that O-GlcNAcylation and its cycling enzymes might be under precise control to ensure successful mitosis.

Mitotic defects in *OGA*$^{-/-}$ *MEFs*

To investigate how constitutively increased O-GlcNAcylation by OGA knockout affected the cell cycle, we next performed flow cytometry analysis with $OGA^{+/+}$ and $OGA^{-/-}$ MEFs. Flow cytometry analysis of DNA content revealed no significant difference between the $OGA^{-/-}$ MEFs and WT MEFs during the early passages (P2). However, during the late passage (P4), $OGA^{-/-}$ MEFs showed increased 4N and decreased 2N fractions compared with $OGA^{+/+}$ MEFs, indicating a partial defect in these stages of the cell cycle (Fig. 5A,B). In addition, flow cytometry analysis of BrdU/PI-stained MEFs showed reduced amounts of G1 and S phase, while G2/M-phase cells increased in the $OGA^{-/-}$ MEFs (Fig. 5C). Downregulation of mitotic regulators such as Aurora and polo-like kinase has been shown to lead to defective mitosis (Kunitoku *et al.*, 2003; Glotzer, 2005; Raouf *et al.*, 2005). Therefore, we examined the protein levels of mitotic regulators and cyclins in $OGA^{-/-}$ MEFs. We found that the protein levels of mitotic regulators such as Aurora Kinase B, cyclin B1, and cdc2 decreased in $OGA^{-/-}$ MEFs, suggesting that the $OGA^{-/-}$ MEFs with 4N DNA have increased nonmitotic (4N-G1) cells. As we observed that OGT was concomitantly changed with cyclin B1 during mitosis in WT cells

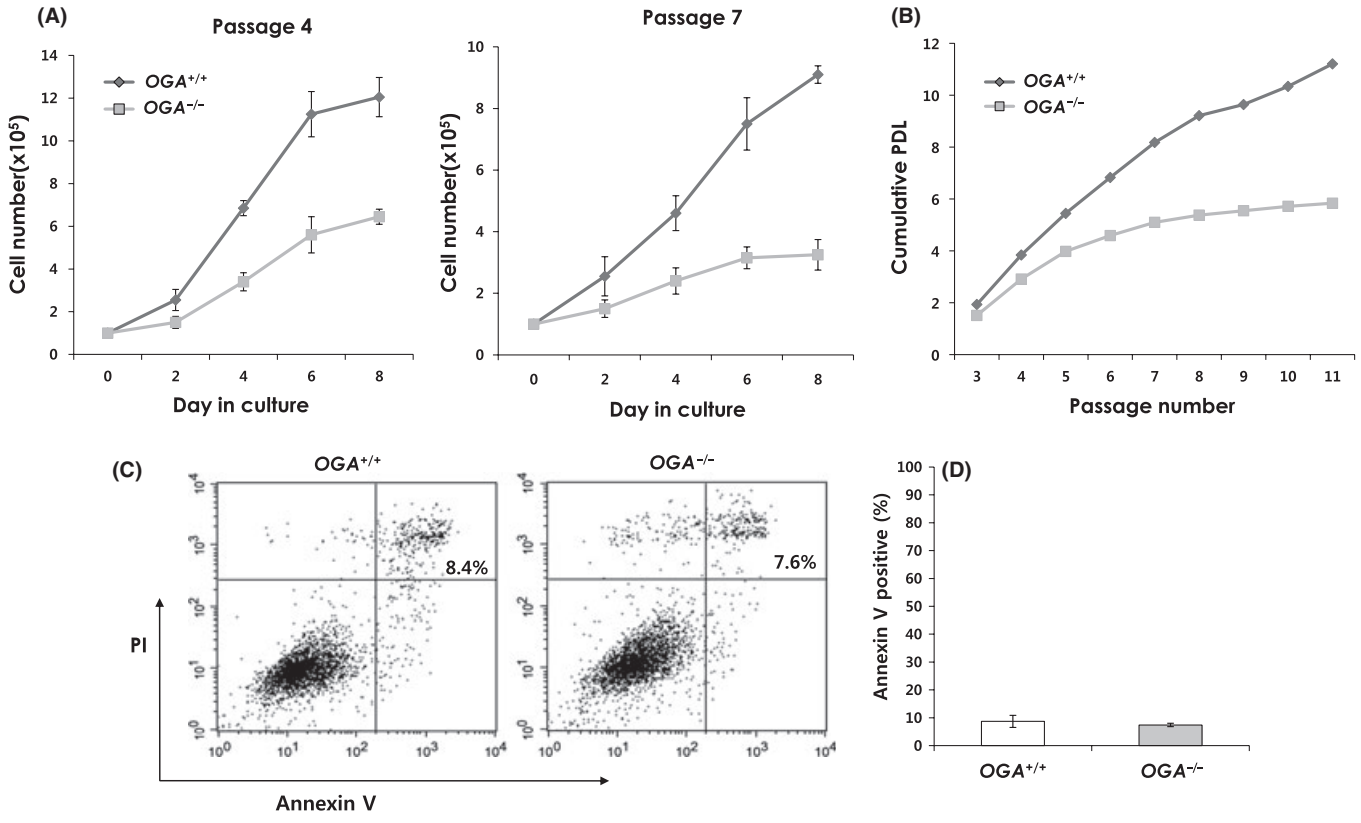

Fig. 3 $OGA^{-/-}$ MEFs exhibit reduced growth rates. (A) Growth curves of $OGA^{+/+}$ and $OGA^{-/-}$ MEFs (passages 4 and 7). Error bars represent the S.D. (n = 3). (B) Growth curves were determined by a 3T3 protocol. $OGA^{+/+}$ and $OGA^{-/-}$ MEFs were seeded on 6-cm culture dishes at a density of 10^5 MEFs every 3 days. (C) The population of apoptotic cells was determined by annexin-V–FITC and propidium iodide (PI) staining. A representative dot plot (left panel) and the mean (right panel) and SD from three independent experiments are presented.

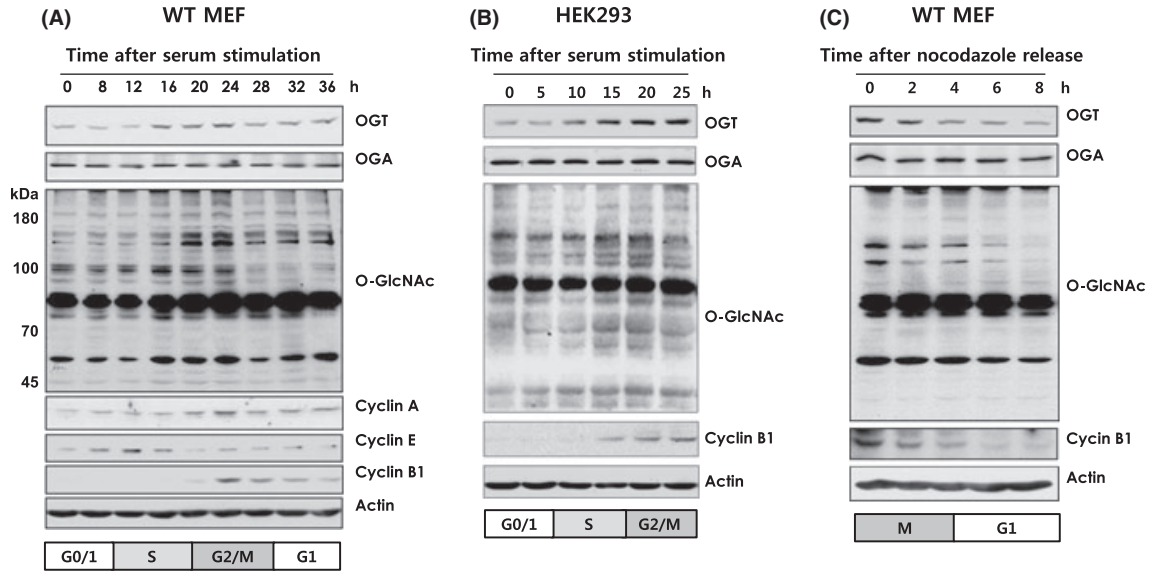

Fig. 4 O-GlcNAcylation fluctuates with OGT expression during cell cycle progression. (A) WT MEFs were arrested in G0 by serum starvation and then stimulated by serum. Total lysates were analyzed at the indicated time point after serum stimulation. Immunodetection in total lysates of the indicated cyclins, O-GlcNAc cycling enzymes, and O-GlcNAc was conducted. (B) The same experiment was performed in HEK293 cells. (C) The indicated proteins from total lysates of WT MEFs at the indicated time points after release from nocodazole were analyzed by Western blotting. Actin was used as a loading control.

(Fig. 4A–C), OGT was also downregulated in $OGA^{-/-}$ MEFs (Fig. 5D). Together, these results suggest that precise control of O-GlcNAcylation is required for cell cycle progression.

Defects in the maintenance of genomic stability

We observed an increase in the percentage of multinucleated cells (>4n) in $OGA^{-/-}$ MEFs, suggesting gain and loss of chromosomes (Fig. 5B). These results prompted us to examine the abnormal nuclear morphologies in $OGA^{-/-}$ MEFs. The WT and $OGA^{-/-}$ MEFs were fixed and stained with Hoechst for nuclei visualization. We observed frequent enlarged nuclei and a high incidence of multinuclear cells in $OGA^{-/-}$ MEFs as compared to $OGA^{+/+}$ (Fig. 6A). $OGA^{-/-}$ MEFs contained a significantly higher number of polynucleated cells (24% of $OGA^{-/-}$ cells vs. 9% $OGA^{+/+}$ cells) and micronuclei (15% of $OGA^{-/-}$ cells vs. 4.8% $OGA^{+/+}$ cells) compared with WT MEFs (Fig. 6B,C). Micronuclei originate from lagging chromosomes and are stably maintained in cells. We next examined whether OGA loss led to mitotic abnormalities, including lagging chromosomes. Indeed, we observed more anaphase figures with lagging chromosomes in $OGA^{-/-}$ MEFs than in $OGA^{+/+}$ MEFs (Fig. 6D). Quantification of the lagging chromosomes is shown Fig. 6E. These results suggest that OGA loss can cause chromosome aberrations marked with nuclear enlargement and aneuploidy. To further confirm the genomic instability in $OGA^{-/-}$ MEFs, we performed chromosome counts on colcemid-arrested metaphase spreads from $OGA^{+/+}$ and $OGA^{-/-}$ MEFs at P5. In $OGA^{-/-}$ MEFs, a higher percentage of cells exhibited abnormal chromosome numbers than in $OGA^{+/+}$ MEFs. These results indicate that the loss of OGA can lead to a loss or gain of a single chromosome (Fig. 6F,G).

Cytokinesis failure in $OGA^{-/-}$ MEFs

Polyploidy can result from cytokinesis failure, which subsequently leads to chromosome instability (Stenmark & Sagona, 2010). OGT and OGA are localized to the midbody and regulate mitotic regulators during cytokinesis (Slawson *et al.*, 2008; Wang *et al.*, 2010). Therefore, we next examined whether the OGA loss impaired cytokinesis. $OGA^{-/-}$ MEFs were monitored by time-lapse differential interference contrast (DIC) microscopy. As expected, the WT MEFs underwent normal cytokinesis. Forty-seven of 53 $OGA^{+/+}$ MEFs exhibited normal cell cleavage and complete separation of the two daughter cells (Fig. 6H,J). In contrast, 18 of 53 $OGA^{-/-}$ MEFs failed to complete cytokinesis and resulted in binucleated cells (Fig. 6I,J). $OGA^{-/-}$ MEFs entered mitosis normally. As shown in Fig. 6I, however, $OGA^{-/-}$ MEFs spent a much longer time in mitotic cell rounding during mitosis compared with WT MEFs.

Cells deficient in mitotic checkpoint regulators commonly display higher rates of polyploidy (Holland & Cleveland, 2009). To assess the possibility of mitotic checkpoint defects in $OGA^{-/-}$ cells, we treated WT and $OGA^{-/-}$ MEFs with nocodazole and analyzed the mitotic defect. However, propidium iodide (PI) staining after nocodazole treatment did not reveal a difference in the fraction of 4N and 8N DNA content between WT and $OGA^{-/-}$ MEFs (Fig. S4A). We also obtained the same results from the knockdown of OGA with shRNA (Fig. S4B). These observations suggest that OGA is necessary for successful completion of cytokinesis.

Together, these findings support a critical role for O-GlcNAc cycling in the maintenance of genomic stability. These results also indicate that OGA dysfunction might contribute to genomic instability linked to the aging process, as we observed increased O-GlcNAcylation and decreased protein levels of OGA and OGT in natural aging.

Discussion

In this study, we found higher levels of O-GlcNAcylation and lower levels of O-GlcNAc cycling enzymes in older mice compared with younger ones in diverse tissues. We investigated how constitutively elevated O-GlcNAcylation affects physiological processes and cellular functions by generating OGA knockout mice. OGA homozygous null embryos exhibited delayed embryonic development and died soon after birth as a result of respiratory failure. $OGA^{-/-}$ MEFs had a reduced growth rate that led to senescence caused by mitotic defects. We also showed that OGA loss led to abnormal chromosome segregation and frequently failed to complete

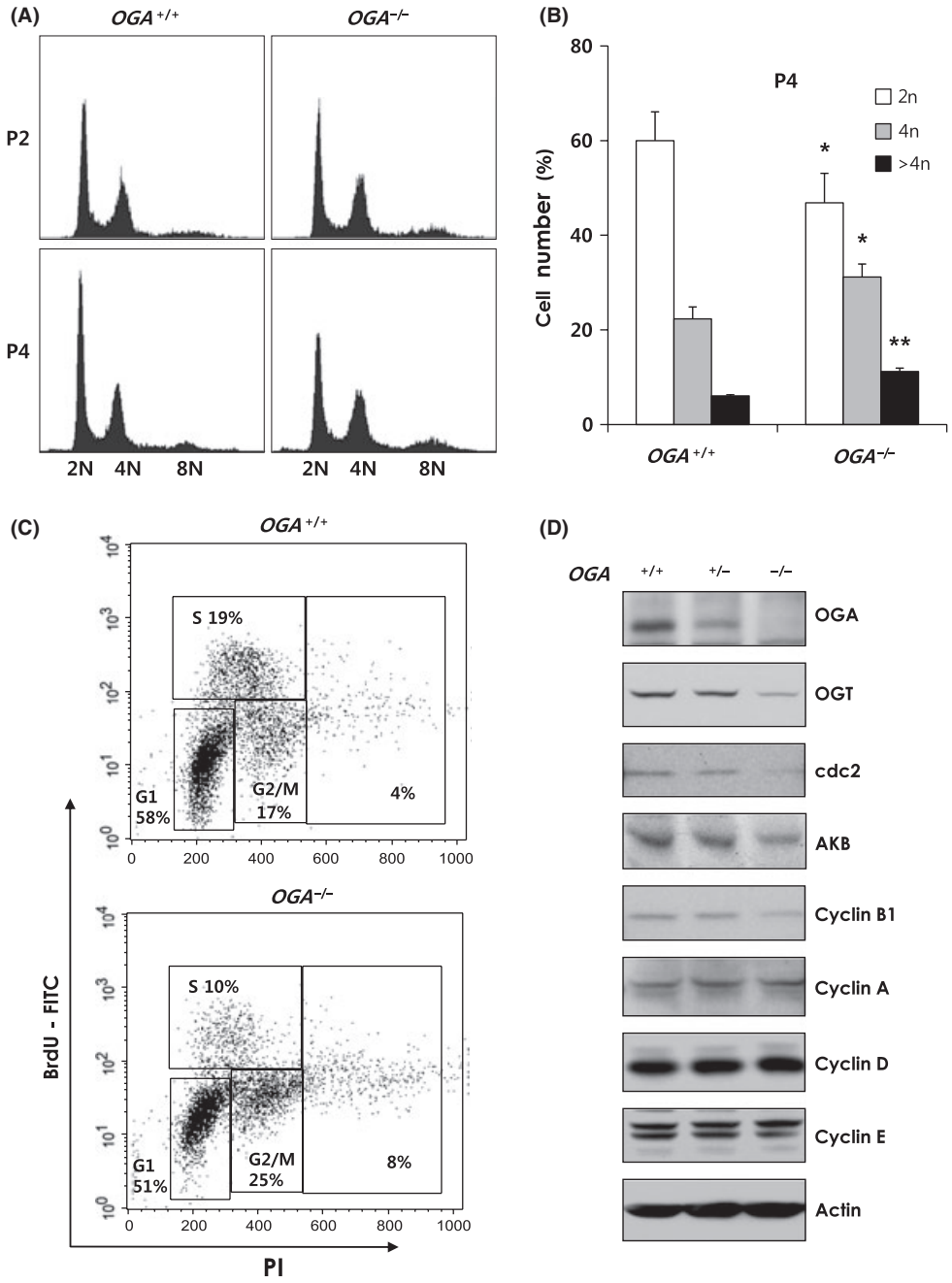

Fig. 5 *OGA*$^{-/-}$ MEFs show mitotic defects and downregulation of mitotic regulators. (A) DNA content profile of asynchronous *OGA*$^{+/+}$ and *OGA*$^{-/-}$ MEFs (P2 and P4). (B) The percentage of cells (P4) in each phase of the cell cycle is shown. Error bars represent the S.D. ($n = 3$) and $^{**}P < 0.005$, $^{*}P < 0.05$ vs. *OGA*$^{+/+}$ MEFs (Student's *t*-test). (C) Cell cycle status of MEFs (P4) analyzed by FACS after BrdU and PI staining. (D) Western blot analysis of the expression levels of OGT, cdc2, AKB, cyclin B1, cyclin A, cyclin D, and cyclin E. Anti-β-actin antibody was used as loading control.

cytokinesis, which ultimately caused aneuploidy. These cellular defects are likely causes of the delayed *OGA*$^{-/-}$ embryo growth and consequent death.

It has studied the important roles of O-GlcNAc cycling during cell cycle. Inhibition of OGA or overexpression of OGT delays M-phase progression in mammalian cells (Slawson *et al.*, 2005). Importantly, O-GlcNAc level is elevated in M phase during *Xenopus laevis* oocytes maturation (Lefebvre *et al.*, 2004; Dehennaut *et al.*, 2009). Consistently, dysregulation of O-GlcNAc cycling impairs cell cycle progression in *Xenopus laevis* oocytes (Dehennaut *et al.*, 2007). We observed that the O-GlcNAcylation level increased at late S phase and peaked at M phase, concomitant with increased OGT levels in mammalian cells. O-GlcNAcylation decreased during mitotic exit, which is controlled by OGA enzymatic activity (Fig. 4A–C). Thus, OGA disruption may profoundly affect multiple mitotic signaling circuits. Consequently, *OGA*$^{-/-}$ MEFs failed to maintain genomic stability, followed by abnormal chromosome segregation and cytokinesis failure. Similarly, a previous study shows that increased O-GlcNAc level by OGT overexpression leads to polyploid nuclei (Slawson *et al.*,

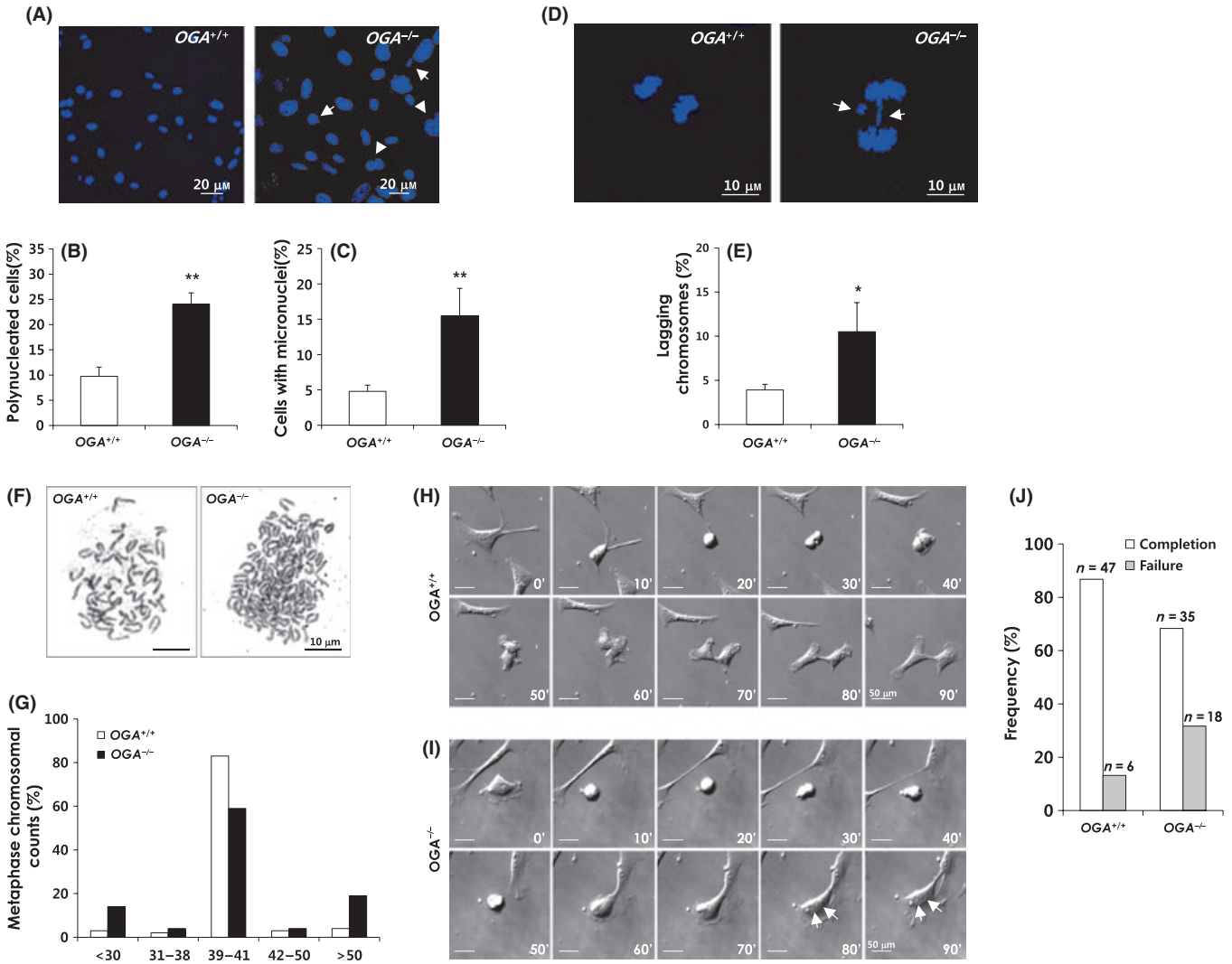

Fig. 6 OGA loss causes genomic instability, and OGA is required for completion of cytokinesis. MEFs were fixed and stained with Hoechst. (A) $OGA^{-/-}$ MEFs had higher numbers of binuclear cells and larger mononuclei and micronuclei compared with $OGA^{+/+}$ MEFs (arrows indicate micronuclei, arrowheads denote binuclear cells). The percentage of polynucleated cells (B) and micronuclei (C) in $OGA^{+/+}$ *and* $OGA^{-/-}$ MEFs. (D) $OGA^{-/-}$ MEFs with a lagging chromosome in anaphase (arrows highlight a lagging chromosome). (E) Quantification of lagging chromosomes in $OGA^{+/+}$ and $OGA^{-/-}$ MEFs. (F) Representative photomicrographs of Giemsa-stained metaphase spreads of $OGA^{+/+}$ *and* $OGA^{-/-}$ MEFs (P5). (G) Metaphase spreading profiles of $OGA^{+/+}$ and $OGA^{-/-}$ MEFs. At least 80 cells were analyzed per genotype per experiment. In all panels, error bars represent the SD and $^{**}P < 0.005$, $^{*}P < 0.02$ (Student's *t*-test). (H and I) Time-lapse DIC images of $OGA^{+/+}$ (H) and $OGA^{-/-}$ (I) MEFs. $OGA^{-/-}$ MEFs displayed cytokinesis failure, resulting in multinucleation (arrows indicate nuclei, time points are in minutes), with scale bars of 50 μm. (J) Frequency of $OGA^{+/+}$ and $OGA^{-/-}$ MEFs that failed to complete cytokinesis.

2005). These results suggest that increased O-GlcNAcylation by OGA disruption or OGT overexpression causes defective mitosis.

Many mitotic regulators of O-GlcNAcylation have been identified. OGA and OGT localizes in a transient complex with vimentin (a cytoskeletal protein), Aurora kinase B (AKB), and protein phosphatase 1 (PP1) at the midbody during cytokinesis, which cooperatively regulates the post-translational status of proteins (Slawson *et al.*, 2008). Nup153 and EMSY, which are required for nuclear envelope breakdown and maintenance of genomic stability, respectively, are also O-GlcNAcylated during M phase (Favreau *et al.*, 1996; Hughes-Davies *et al.*, 2003; Raouf *et al.*, 2005; Ullman *et al.*, 2009; Wang *et al.*, 2010). Furthermore, nuclear mitotic apparatus protein 1 (NuMA1) plays an important role in spindle pole formation and is O-GlcNAcylated at M phase (Silk *et al.*, 2009; Yokomori *et al.*, 2009; Wang *et al.*, 2010). OGT overexpression causes inhibitory phosphorylation of CDK1 and consequently reduces the phosphorylation of CDK1 target proteins (Wang *et al.*, 2010). However, how O-GlcNAcylation controls specific mitotic regulators during mitosis has not been demonstrated. These data suggest that the precise control of O-GlcNAcylation on mitotic regulators is critical for mitosis.

In addition to genomic instability, epigenetic changes are a critical component of aging in all eukaryotes. The potential roles of O-GlcNAcylation in epigenetic regulation have been investigated. O-GlcNAcylation occurs on nuclear pores and many nuclear and chromatin-associated proteins. Many transcription factors are O-GlcNAcylated, which affects their transcriptional activity (Ozcan *et al.*, 2010). In addition, O-GlcNAc cycling can affect the activity of RNA polymerase II (Kelly *et al.*, 1993; Hart & Comer, 2001). Strikingly, recent studies have shown that histones H2A, H2B, and H4 are O-GlcNAcylated within the nucleosome core, implicating an

important role for O-GlcNAc in chromatin remodeling and epigenetic regulation (Sakabe & Hart, 2010; Sakabe *et al.*, 2010). Correlatively, the *ogt-1* and *oga-1* null mutant alleles of *Caenorhabditis elegans* show that disruption of O-GlcNAc cycling leads to age-related transcriptional changes (Love *et al.*, 2010). These results also support the close relationship between the aging process and dysregulation of O-GlcNAcylation. This evidence and our results suggest that increased O-GlcNAcylation by aberrant regulation of O-GlcNAc cycling enzymes might lead to epigenetic changes that contribute to natural aging.

Because genomic instability is a hallmark of most cancers, our results raise the possibility that OGA or OGT is dysfunctional in cancer. Consistent with this idea, dysregulation of O-GlcNAcylation and aberrant protein levels of O-GlcNAc cycling enzymes are observed in tumors and in cancer cell lines. In breast tissue or thyroid cancers, decreased O-GlcNAc levels and increased OGA enzymatic activity occur (Slawson *et al.*, 2001; Krzeslak *et al.*, 2010). In contrast, however, many studies have recently shown increases in the O-GlcNAc levels and the protein levels of O-GlcNAc cycling enzymes in cancers. Lung and colon tissue exhibited increased O-GlcNAcylation and protein levels of O-GlcNAc cycling enzymes (Gu *et al.*, 2010; Yu *et al.*, 2011). Moreover, in patients with chronic lymphocytic leukemia, O-GlcNAcylated proteins increased, and the protein levels of O-GlcNAc cycling enzymes also increased (Shi *et al.*, 2010). In breast cancer cell lines, O-GlcNAc levels are elevated, and the OGT level also increases compared with less aggressive breast cancer lines. Importantly, OGT knockdown in breast cancer cells inhibits tumor growth both an *in vitro* and in an *in vivo* mouse model (Caldwell *et al.*, 2010). OGT deficiency in a mammalian model reveals that OGT is essential for stem cell viability (Shafi *et al.*, 2000). Moreover, the tissue-specific OGT knockout using floxed mice leads to T-cell apoptosis and fibroblast growth arrest (O'Donnell *et al.*, 2004). We show here that $OGA^{-/-}$ MEF exhibited reduced growth with a decreased OGT level. Similarly, OGT disruption also leads to a parallel decrease in OGA protein levels (Kazemi *et al.*, 2010). OGT knockdown cells by shRNA also displayed a reduced OGA level and decreased growth rate (Fig. S3A,B). These results reflect the observation that many cases of cancer tissues display increased protein levels of O-GlcNAc cycling enzymes, while aged tissues show decreased protein levels of O-GlcNAc cycling enzymes. Thus, we propose that aberrantly increased protein levels of O-GlcNAc cycling enzymes might be critical for cancer cell growth rather than total O-GlcNAcylation change.

In summary, this study provides key insight into the role of OGA in the maintenance of genomic instability linked to aging. OGA loss caused a reduced growth rate and cellular senescence with genomic instability. OGA enzymatic activity is important to complete mitosis with OGT functions. Abnormal OGA function might contribute to the aging process and be associated with development of age-related chronic diseases.

Materials and methods

Histology

For the histological analysis, mouse embryos, placentas, and tissues were collected, fixed with 10% phosphate-buffered formalin, dehydrated, and embedded in paraffin. The 6-μm sections were stained with hematoxylin and eosin by standard procedures. The slides were observed under a digital virtual microscope (dotSlide; Olympus, Tokyo, Japan).

Generation of MEFs and growth rate analysis

MEFs were isolated from 12.5 to 14.5 dpc embryos. After removal of the intestinal organs and head, embryos were washed with phosphate-buffered saline (PBS), minced, and trypsinized. After centrifugation, the dissociated cells were plated in Dulbeccos's modified Eagle's medium (DMEM) containing 10% fetal bovine serum. Growth curves were determined at passages 4 and 6. At day 0, 10^5 MEFs were seeded in triplicate on 6-cm plates, counted, and reseeded at the same density every 2–3 days. The population-doubling rate of each passage was calculated using a log2 formula (the number of harvested cells/the number of seeded cells).

Apoptosis assays using annexin-V and PI

$OGA^{+/+}$ and $OGA^{-/-}$ MEFs were harvested, washed with ice-cold PBS, and resuspended in annexin-V binding buffer. Annexin-V–FITC (BD Biosciences, San Jose, CA, USA) and PI (Sigma, St. Louis, MO, USA) were added to the cells and incubated for 15 min at room temperature in the dark. Samples were analyzed by FACSCalibur (BD Biosciences).

Western blotting and immunofluorescence staining analysis

Tissue and cell lysates were prepared using standard procedures. Samples of 20–30 μg of protein were separated on an SDS-polyacrylamide gel and visualized. Western blotting antibodies used were anti-cyclin A (sc-596; Santa Cruz Biotechnology, Santa Cruz, CA, USA), anti-cyclin B1 (05-158; Upstate Biotechnology, Lake Placid, NY, USA), anti-cyclin E (sc-481; Santa Cruz Biotechnology), anti-cyclin D (sc-450; Santa Cruz Biotechnology), anti-AKB (611082; BD Biosciences), anti-cdc2 (9112; Cell Signaling Technology, Beverly, MA, USA), and β-actin (691001; MP Biomedicals, Santa Ana, CA, USA). The antibodies used for the anti-O-GlcNAc Western blots (CTD110.6) were kindly provided by Dr. Gerald Hart (Johns Hopkins University, Baltimore, MD, USA). Anti-OGT and OGA polyclonal antibodies had been previously generated and were used as previously described (Suh *et al.*, 2008). Synthetic peptides (YAAGNKPDHMIK) for the anti-OGT antibody and purified His-OGA protein for the anti-OGA antibody were conjugated with keyhole limpet hemocyanin (KLH) (Calbiochem, San Diego, CA, USA) using glutaraldehyde. The peptide–KLH conjugates were immunized into a New Zealand white rabbit. The peroxidase-labeled goat anti-mouse IgG and the goat anti-mouse IgA, IgM, and IgG used as the secondary antibodies were obtained from Kirkegaard & Perry Laboratories (KPL, Gaithersburg, MD, USA).

For nuclei staining, the MEFs were grown on coverslips, fixed for 15 min at room temperature in 4% paraformaldehyde, and washed in PBS. DNA was visualized with Hoechst stain (Sigma), and the coverslips were mounted on slides. Nuclei were analyzed using a FV1000SPD (Olympus).

Cell cycle study

For primary MEF asynchronous cell cycle analysis, bromodeoxyuridine (BrdU) and PI staining was performed using BrdU flow kits (BD Pharmingen, San Diego, CA, USA). Briefly, the MEFs were incubated with 10 μM BrdU for 4 h. After harvesting and fixation, cells were permeabilized with BD Cytofix/Cytoperm™ buffer (BD Biosciences) and were labeled with an FITC-conjugated anti-BrdU antibody. Total DNA was stained with PI solution and analyzed using a FACSCalibur instrument (BD Biosciences).

Cytogenetic analyses

MEFs were treated with 0.1 μg mL^{-1} colcemid (Gibco/BRL, Grand Island, NY, USA) for 5 h. After washing with PBS, the cells were detached and incubated in 0.075 M KCl (hypotonic solution) at 37 °C for 15 min. The

cells were fixed with methanol/glacial acetic acid (3:1) three times at room temperature for 10 min. The cells were dropped on a slide and stained with Giemsa.

Live cell imaging

Asynchronously grown MEFs were seeded on coverslips and maintained in a heated culture chamber (37 °C, 5% CO_2) on Microscope equipped with a CO_2 control system and a humidity chamber. The cells were visualized by DIC imaging. DIC images were collected at 10-min intervals for 24 h. Live images of cell division were obtained using an IX81-ZDC in UNIST-Olympus Biomed Imaging Center (UOBC).

Acknowledgments

This work was supported by the National Research Foundation of Korea Grant funded by the Korean Government (KRF-2007-341-C00027), a grant from the Korean Ministry of Education, Science and Technology (The Regional Core Research Program/Anti-aging and Well-being Research Center), the National Research Foundation of Korea Grant funded by the Korean government (no. 2010-0029434), and the Fusion Pioneer Project (PGB013) from the National Research Foundation of Korea.

References

Caldwell SA, Jackson SR, Shahriari KS, Lynch TP, Sethi G, Walker S, Vosseller K, Reginato MJ (2010) Nutrient sensor O-GlcNAc transferase regulates breast cancer tumorigenesis through targeting of the oncogenic transcription factor FoxM1. *Oncogene* **29**, 2831–2842.

Capotosti F, Guernier S, Lammers F, Waridel P, Cai Y, Jin J, Conaway JW, Conaway RC, Herr W (2011) O-GlcNAc transferase catalyzes site-specific proteolysis of HCF-1. *Cell* **144**, 376–388.

Glotzer M (2005) The molecular requirements for cytokines. *Science* **307**, 1735–1739.

Dehennaut V, Lefebvre T, Sellier C, Leroy Y, Gross B, Walker S, Cacan R, Michalski JC, Vilain JP, Bodart JF (2007) O-linked N-acetylglucosaminyltransferase inhibition prevents G2/M transition in Xenopus laevis oocytes. *J. Biol. Chem.* **282**, 12527–12536.

Dehennaut V, Lefebvre T, Leroy Y, Vilain JP, Michalski JC, Bodart JF (2009) Survey of O-GlcNAc level variations in Xenopus laevis from oogenesis to early development. *Glycoconj. J.* **26**, 301–311.

Dimri GP, Lee XH, Basile G, Acosta M, Scott C, Roskelley C, Medrano EE, Linskens M, Rubelj I, Pereirasmith O, Peacocke M, Campisi J (1995) A biomarker that identifies senescent human-cells in culture and in aging skin *in-vivo*. *Proc. Natl. Acad. Sci. USA* **92**, 9363–9367.

Draviam VM, Xie S, Sorger PK (2004) Chromosome segregation and genomic stability. *Curr. Opin. Genet. Dev.* **14**, 120–125.

Favreau C, Worman HJ, Wozniak RW, Frappier T, Courvalin JC (1996) Cell cycle-dependent phosphorylation of nucleoporins and nuclear pore membrane protein Gp210. *Biochemistry* **35**, 8035–8044.

Gu Y, Mi W, Ge Y, Liu H, Fan Q, Han C, Yang J, Han F, Lu X, Yu W (2010) GlcNAcylation plays an essential role in breast cancer metastasis. *Cancer Res.* **70**, 6344–6351.

Hart GW, Comer FI (2001) Reciprocity between O-GlcNAc and O-phosphate on the carboxyl terminal domain of RNA polymerase II. *Biochemistry* **40**, 7845–7852.

Hart GW, Housley MP, Slawson C (2007) Cycling of O-linked beta-N-acetylglucosamine on nucleocytoplasmic proteins. *Nature* **446**, 1017–1022.

Hart GW, Slawson C, Ramirez-Correa G, Lagerlof O (2010) Cross talk between O-GlcNAcylation and phosphorylation: roles in signaling, transcription, and chronic disease. *Annu. Rev. Biochem.* **80**, 825–858.

Holland AJ, Cleveland DW (2009) Boveri revisited: chromosomal instability, aneuploidy and tumorigenesis. *Nat. Rev. Mol. Cell Biol.* **10**, 478–487.

Hughes-Davies L, Huntsman D, Ruas M, Fuks F, Bye J, Chin SF, Milner J, Brown LA, Hsu F, Gilks B, Nielsen T, Schulzer M, Chia S, Ragaz J, Cahn A, Linger L, Ozdag H, Cattaneo E, Jordanova ES, Schuuring E, Yu DS, Venkitaraman A, Ponder B, Doherty A, Aparicio S, Bentley D, Theillet C, Ponting CP, Caldas C, Kouzarides T (2003) EMSY links the BRCA2 pathway to sporadic breast and ovarian cancer. *Cell* **115**, 523–535.

Kazemi Z, Chang H, Haserodt S, McKen C, Zachara NE (2010) O-linked beta-N-acetylglucosamine (O-GlcNAc) regulates stress-induced heat shock protein expression in a GSK-3beta-dependent manner. *J. Biol. Chem.* **285**, 39096–39107.

Kelly WG, Dahmus ME, Hart GW (1993) RNA polymerase II is a glycoprotein. Modification of the COOH-terminal domain by O-GlcNAc. *J. Biol. Chem.* **268**, 10416–10424.

Krzeslak A, Pomorski L, Lipinska A (2010) Elevation of nucleocytoplasmic beta-N-acetylglucosaminidase (O-GlcNAcase) activity in thyroid cancers. *Int. J. Mol. Med.* **25**, 643–648.

Kunitoku N, Sasayama T, Marumoto T, Zhang D, Honda S, Kobayashi O, Hatakeyama K, Ushio Y, Saya H, Hirota T (2003) CENP-A phosphorylation by Aurora-A in prophase is required for enrichment of Aurora-B at inner centromeres and for kinetochore function. *Dev. Cell* **5**, 853–864.

Lefebvre T, Baert F, Bodart JF, Flament S, Michalski JC, Vilain JP (2004) Modulation of O-GlcNAc glycosylation during Xenopus oocyte maturation. *J. Cell Biochem.* **93**, 999–1010.

Lehman DM, Fu DJ, Freeman AB, Hunt KJ, Leach RJ, Johnson-Pais T, Hamlington J, Dyer TD, Arya R, Abboud H, Goring HHH, Duggirala R, Blangero J, Konrad RJ, Stern MP (2005) A single nucleotide polymorphism in MGEA5 encoding O-GlcNAc-selective N-acetyl-beta-D glucosaminidase is associated with type 2 diabetes in Mexican Americans. *Diabetes* **54**, 1214–1221.

Love DC, Ghosh S, Mondoux MA, Fukushige T, Wang P, Wilson MA, Iser WB, Wolkow CA, Krause MW, Hanover JA (2010) Dynamic O-GlcNAc cycling at promoters of Caenorhabditis elegans genes regulating longevity, stress, and immunity. *Proc. Natl. Acad. Sci. USA* **107**, 7413–7418.

O'Donnell N, Zachara NE, Hart GW, Marth JD (2004) Ogt-dependent X-chromosome-linked protein glycosylation is a requisite modification in somatic cell function and embryo viability. *Mol. Cell. Biol.* **24**, 1680–1690.

Ozcan S, Andrali SS, Cantrell JE (2010) Modulation of transcription factor function by O-GlcNAc modification. *Biochim. Biophys. Acta* **1799**, 353–364.

Rajamani U, Essop MF (2010) Hyperglycemia-mediated activation of the hexosamine biosynthetic pathway results in myocardial apoptosis. *Am. J. Physiol. Cell Physiol.* **299**, C139–C147.

Raouf A, Brown L, Vrcelj N, To K, Kwok W, Huntsman D, Eaves CJ (2005) Genomic instability of human mammary epithelial cells overexpressing a truncated form of EMSY. *J. Natl. Cancer Inst.* **97**, 1302–1306.

Sakabe K, Hart GW (2010) O-GlcNAc transferase regulates mitotic chromatin dynamics. *J. Biol. Chem.* **285**, 34460–34468.

Sakabe K, Wang Z, Hart GW (2010) Beta-N-acetylglucosamine (O-GlcNAc) is part of the histone code. *Proc. Natl. Acad. Sci. USA* **107**, 19915–19920.

Shafi R, Iyer SP, Ellies LG, O'Donnell N, Marek KW, Chui D, Hart GW, Marth JD (2000) The O-GlcNAc transferase gene resides on the X chromosome and is essential for embryonic stem cell viability and mouse ontogeny. *Proc. Natl. Acad. Sci. USA* **97**, 5735–5739.

Shi Y, Tomic J, Wen F, Shaha S, Bahlo A, Harrison R, Dennis JW, Williams R, Gross BJ, Walker S, Zuccolo J, Deans JP, Hart GW, Spaner DE (2010) Aberrant O-GlcNAcylation characterizes chronic lymphocytic leukemia. *Leukemia* **24**, 1588–1598.

Silk AD, Holland AJ, Cleveland DW (2009) Requirements for NuMA in maintenance and establishment of mammalian spindle poles. *J. Cell Biol.* **184**, 677–690.

Slawson C, Pidala J, Potter R (2001) Increased N-acetyl-beta-glucosaminidase activity in primary breast carcinomas corresponds to a decrease in N-acetylglucosamine containing proteins. *Biochim. Biophys. Acta* **1537**, 147–157.

Slawson C, Zachara NE, Vosseller K, Cheung WD, Lane MD, Hart GW (2005) Perturbations in O-linked beta-N-acetylglucosamine protein modification cause severe defects in mitotic progression and cytokinesis. *J. Biol. Chem.* **280**, 32944–32956.

Slawson C, Lakshmanan T, Knapp S, Hart GW (2008) A mitotic GlcNAcylation/phosphorylation signaling complex alters the posttranslational state of the cytoskeletal protein vimentin. *Mol. Biol. Cell* **19**, 4130–4140.

Stenmark H, Sagona AP (2010) Cytokinesis and cancer. *FEBS Lett.* **584**, 2652–2661.

Stryke D, Kawamoto M, Huang CC, Johns SJ, King LA, Harper CA, Meng EC, Lee RE, Yee A, L'Italien L, Chuang PT, Young SG, Skarnes WC, Babbitt PC, Ferrin TE (2003) BayGenomics: a resource of insertional mutations in mouse embryonic stem cells. *Nucleic Acids Res.* **31**, 278–281.

Suh PG, Song M, Kim HS, Parka JM, Kim SH, Kim IH, Ryu SH (2008) O-GlcNAc transferase is activated by CaMKIV-dependent phosphorylation under potassium chloride-induced depolarization in NG-108-15 cells. *Cell Signal.* **20**, 94–104.

Toleman C, Paterson AJ, Whisenhunt TR, Kudlow JE (2004) Characterization of the histone acetyltransferase (HAT) domain of a bifunctional protein with activable O-GlcNAcase and HAT activities. *J. Biol. Chem.* **279**, 53665–53673.

Torres CR, Hart GW (1984) Topography and polypeptide distribution of terminal N-acetylglucosamine residues on the surfaces of intact lymphocytes. Evidence for O-linked GlcNAc. *J. Biol. Chem.* **259**, 3308–3317.

Ullman KS, Mackay DR, Elgort SW (2009) The nucleoporin Nup153 has separable roles in both early mitotic progression and the resolution of mitosis. *Mol. Biol. Cell* **20**, 1652–1660.

Wang Z, Udeshi ND, Slawson C, Compton PD, Sakabe K, Cheung WD, Shabanowitz J, Hunt DF, Hart GW (2010) Extensive crosstalk between O-GlcNAcylation and phosphorylation regulates cytokinesis. *Sci. Signal.* **3**, ra2.

Webster DM, Teo CF, Sun Y, Wloga D, Gay S, Klonowski KD, Wells L, Dougan ST (2009) O-GlcNAc modifications regulate cell survival and epiboly during zebrafish development. *BMC Dev. Biol.* **9**, 28.

Yokomori K, Kong XD, Ball AR, Sonoda E, Feng J, Takeda S, Fukagawa T, Yen TJ (2009) Cohesin associates with spindle poles in a mitosis-specific manner and functions in spindle assembly in vertebrate cells. *Mol. Biol. Cell* **20**, 1289–1301.

Yu WG, Mi WY, Gu YC, Han CF, Liu HY, Fan QO, Zhang XL, Cong Q (2011) O-GlcNAcylation is a novel regulator of lung and colon cancer malignancy. *Bba-Mol Basis Dis.* **1812**, 514–519.

Supporting Information

Additional supporting information may be found in the online version of this article:

Data S1. Methods.

Fig. S1 Generation of *OGA*$^{-/-}$ mice and confirmation of gene trap vector insertion in the *OGA* gene. (A) A gene-trapping vector was used to disrupt OGA. (B) The gene trap vector was inserted in the first intron. (C) PCR genotyping of tails was used to confirm the status of *OGA*$^{+/+}$ *and OGA*$^{+/}$ mice. The indicated primers (F, R, and T) were used in genotyping. (D) Whole-mount lacZ staining of E10.5 and E12.5 embryos and placentas, confirming the insertion of gene trap beta-galactosidase reporter alleles.

Fig. S2 OGA expression during mouse development. Sagittal section of embryos (A) and radial sections of placenta (B) stained with X-gal at stage E14.5. Ma, maternal decidua; Sp, syncytiotrophoblast layer; TG, trophoblast giant cell layer; La, labyrinthine layer.

Fig. S3 Reduced growth rate in OGA and OGT knockdown cell lines. (A) Western blots confirming the shRNA knockdown of OGA and OGT in total lysates from stable cell lines. (B) Growth curves of the control vector, OGA, and OGT knockdown HEK293 cells. Error bars represent the S.D.

Fig. S4 OGA loss does not affect the mitotic checkpoint defect. (A) Cell cycle analysis by flow cytometry of *OGA*$^{+/+}$ *and OGA*$^{-/-}$ MEFs treated with nocodazole (100 ng mL^{-1}) for the indicated number of hours. (B) The experiment was performed with OGA knockdown and control cell lines.

As a service to our authors and readers, this journal provides supporting information supplied by the authors. Such materials are peer-reviewed and may be re-organized for online delivery, but are not copy-edited or typeset. Technical support issues arising from supporting information (other than missing files) should be addressed to the authors.